Hyperbranched Polyurethane-Urea-Imide/*o*-Clay-Silica Hybrids: Synthesis and Characterization

Aswini K Mishra,[1] Ramanuj Narayan,[1] Tejraj M. Aminabhavi,[2] S. K. Pradhan,[3] K. V. S. N. Raju[1]

[1]*Organic Coatings and Polymers Division, Indian Institute of Chemical Technology, Hyderabad 500 007, India*
[2]*Soniya Education Trust's College of Pharmacy, S.R. Nagar, Dharwad 580 002, India*
[3]*Advanced Materials Technology Department, Institute of Minerals and Materials Technology (Formerly Regional Research Laboratory), Bhubaneswar, Orissa 751 013, India*

Received 17 March 2011; accepted 23 May 2011
DOI 10.1002/app.34970
Published online 27 December 2011 in Wiley Online Library (wileyonlinelibrary.com).

ABSTRACT: Hyperbranched polyurethane-urea-imide/*o*-clay-silica (HBPUI/*o*-clay-silica) hybrid coatings were prepared using organically modified clay (*o*-clay) in the presence of cetyltrimethylammonium bromide (CTAB) and tributylhexadecylphosphonium bromide (TBHPB) cationic surfactants and were further surface-grafted by 3-aminopropyltrimethoxy silane (APTMS). Hybrid polyesters were prepared by incorporating into the first generation hyperbranched polyester polyol (HBP-G1) at various concentrations. The *NCO*-terminated hybrid prepolymers and chain extensions were achieved by imide chain extender. The modified clays were characterized by powder X-ray diffraction and Fourier transform spectroscopy. Viscoelastic, thermomechanical, and surface topology studies were performed by dynamic mechanical thermal analysis (DMTA), thermogravimetric analyser (TGA), universal testing machine (UTM), atomic force microscopic (AFM), and contact angle measurements. TGA and DMTA indicated higher thermal stability and glass transition temperature (T_g) of TBHPB-modified hybrid coatings compared with the CTAB counterparts, which increased with increasing silane-modified *o*-clay content. Water contact angle suggested increasing hydrophobicity of higher silane-modified *o*-clay containing coatings, while AFM confirmed the dispersibility of silane-modified *o*-clay into polymer matrix; the extent of dispersion increased with increasing silane-modified *o*-clay content in the hybrid formulation. © 2011 Wiley Periodicals, Inc. J Appl Polym Sci 125: E67–E75, 2012

Key words: hyperbranched; polyurethane; hybrid coating; FTIR; TGA

INTRODUCTION

Continuing interests in the development of novel polymeric coatings have led to extensive research efforts.[1–3] This can be achieved either by chemical or structural modification of polymers[4] or by partial replacement of linear structures with dendrimers or hyperbranched polymers (HBPs).[5] In particular, HBPs, because of their ease of synthesis on a large scale at a reasonable cost with excellent flow and processing characteristics possesses higher industrial importance. The properties of HBPs such as lower viscosity, higher solubility, and globular structure with a large number of reactive end groups have been widely explored.[6–8] Innumerable efforts have been made to improve the properties of conventional polyurethane (PU) coatings by incorporating imide functionality into PU backbone[9,10] and partial replacement of linear structures with HBPs.[11,12] The montmorillonite (MMT), layered silicate clay, with lamellar shape, has been used to prepare the various polymer/clay nanocomposites.[13–17] Clay being incompatible with organic polymers, efforts have been made to improve its compatibility with organic networks.[18–29] The properties of such hybrid materials have further been improved by the surface modification of *o*-clay with organosilane coupling agents.[30,31]

Many reports are available on the synthesis and characterization of different polymer/clay nanocomposite coatings. But, very few reports are available on hyperbranched PU hybrid coatings based on 3-aminopropyltrimethoxy silane (APTMS) modified *o*-clay.[32,33] The significance of our work in comparisons with the earlier established work is that in this study, we have focused more on the structure property relation study of different hyperbranched polyurethane-urea-imide (HBPUI) hybrid coatings based on Fourier transform infrared (FTIR) peak deconvolution process what is rarely reported. In this synthetic approach, we have planed to study the effect of the APTMS-modified *o*-clay which contains amine functional groups in the outer surface, on the HBPUI hybrid coating properties. In our study, the clay particles were homogeneously distributed in the polymer matrix because of higher reactivity [confirmed by atomic force microscopy (AFM)] thereby giving better thermomechanical and tensile properties.

Correspondence to: K. V. S. N. Raju (kvsnraju@iict.res.in; drkvsnraju@gmail.com).

© 2011 Wiley Periodicals, Inc.

Thus, these hybrid nanocomposite coatings can be utilized for the development of optically active films, contact lenses, corrosion resistance coating, flame retardancy coating, abrasion resistant coatings, and coil coatings.[34,35] Continuing our earlier research,[29] herein, we have reported the synthesis of different HBPUI/*o*-clay-silica hybrid coatings. To achieve these hybrid coatings, the K10-clay was first modified by different cationic surfactants and was further surface-grafted by APTMS coupling agents. The obtained HBPUI/*o*-clay-silica hybrid coating films were characterized by a variety of techniques.

EXPERIMENTAL

Materials

Tributylhexadecylphosphonium bromide (TBHPB), APTMS, untreated MMT K-10 clay, 4,4′-bis methylene dicyclohexyl diisocyanate (HMDI), and *N*-hydroxyphthalimide were purchased from Aldrich (Milwaukee, WI); hydrochloric acid, cetyltrimethylammonium bromide (CTAB), *N*,*N*′-dimethyl formamide, 1,4-dioxane, and sulfur-free toluene were procured from S.D. fine Chemicals (Mumbai, India). The solvents were freed from moisture using 4Å molecular sieves.

Characterization methods

X-ray diffraction (XRD) spectra were recorded using Siemens/D-5000 diffractometer under *CuK* radiation ($\lambda = 1.5406$Å), while FTIR of pristine, organically modified and siloxane-grafted K10 clay samples were taken using KBr pellets. Mid-infrared spectra were acquired using Thermo Nicolet Nexus 670 spectrometer and each sample was scanned 128 times with a resolution of 4 cm^{-1}. All the spectra were scanned within the range of 400–4000 cm^{-1}.

TGA analyses of *o*-clay and different HBPUI/*o*-clay-silica hybrid samples were obtained using TA Instruments (Model Q500). For the analysis, approximately 10 mg of the sample was heated in a platinum crucible and scanned by a high-resolution TGA instrument operating at ramp 10°C/min from room temperature to 600°C in a high purity flowing nitrogen atmosphere (40 cm^3/min). Viscoelastic behavior of HBPUI/*o*-clay-silica hybrid films in the temperature range 25–200°C was measured by dynamic mechanical thermal analyzed instrument (DMTA-IV, Rheometric Scientific, NJ) in a tensile mode at 1 Hz frequency with a heating rate of 3°C min^{-1}.

The tensile strength of different HBPUI/*o*-clay-silica hybrid films were measured by AGS-10kNG, Shimadzu system connected with Autograph controller/measurement unit. For this, the samples were cut into a dumbbell-shape specimen. The AFM images of different HBPUI/*o*-clay-based hybrid films were recorded on a Dualscope 95-200 instrument (Denmark) in a contact mode.

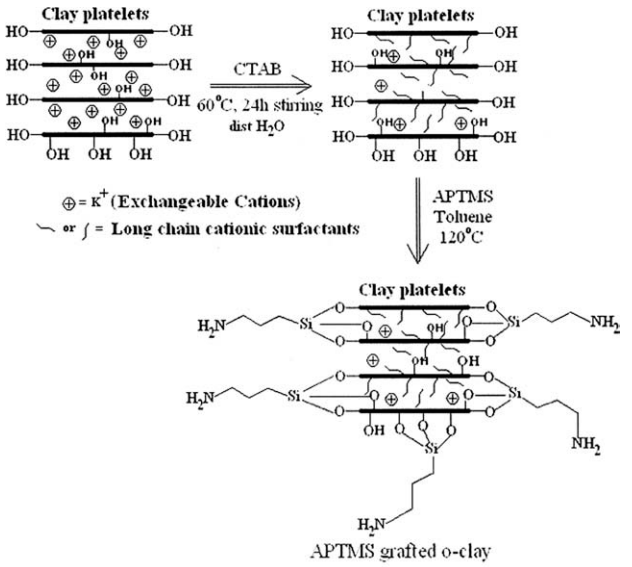

Scheme 1 The schematic outline for clay modification and APTMS grafting onto *o*-clay surface.

Modification K-10 clay and their surface grafting by APTMS

The procedure for clay modification was outlined before[29] and grafting of APTMS onto *o*-clay surface was done according to the earlier described procedure.[36] Initially, 10 g of *o*-clay was dried in a vacuum oven for 24 h, which was dispersed in 500 mL of anhydrous toluene using ultrasonication probe for 30 min and the mixture was further sonicated for another 1 h on a magnetic stirrer. Then APTMS (10 wt %) with catalytic triethylamine was added with stirring under N_2 atmosphere. The mixture was refluxed under N_2 atmosphere for another 6 h, cooled to room temperature, and then the modified clay particles were vacuum filtered with vigorous washing using toluene. The APTMS-grafted *o*-clay particles were collected by continuously extracting through soxhlet using toluene for about 24 h. The nanoparticles were finally dried in a low-pressure oven at 100°C for 24 h and used in the reaction. The detail modification process is shown in Scheme 1. The CTAB and TBHPB surfactant-modified clays are coded as K10-CTAB and K10-TBHPB, while their corresponding silane-modified samples are designated as K10-CTAB-Si and K10-TBHPB-Si, respectively.

Synthesis of HBPUI/o-clay-silica hybrid films

Before the synthesis of HBPUI/*o*-clay-silica hybrid coatings, the silane-grafted *o*-clay was first incorporated into hyperbranched polyester polyol (HBP-G1)

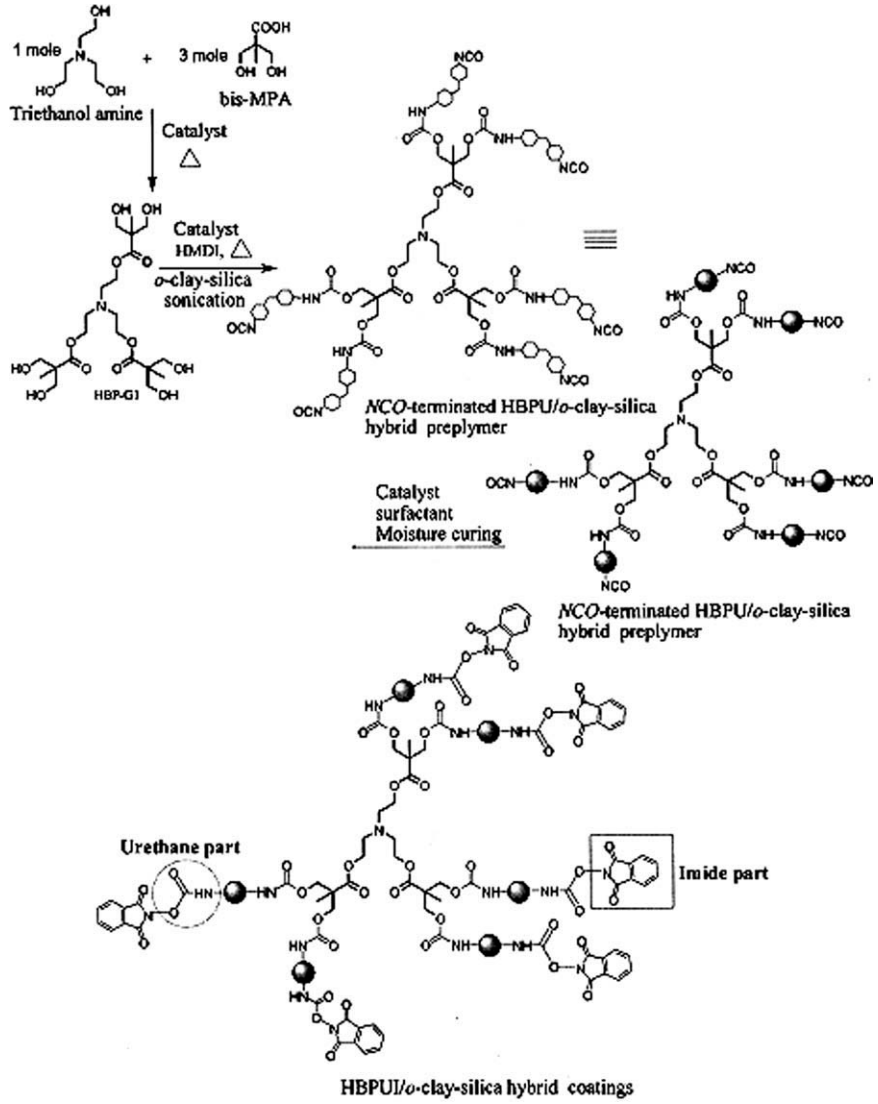

Scheme 2 The outline of the synthetic procedure for HBPUI/*o*-clay-silica hybrid coatings.

matrix at various concentrations through ultrasonication to get different hybrid polyesters. The polyester polyol (HBP-G1) was synthesized by reacting triethanolamine core and bis-MPA in the molar ratio of 1 : 3 by polycondensation process.[37] In the second step, these hybrid polyesters were reacted with HMDI at NCO/OH ratio (1.2 : 1) to get *NCO*-terminated hybrid prepolymers. The excess *NCO* content of the prepolymer was calculated by standard dibutyl amine titration method and was chain extended by *N*-hydroxypthalamide as chain extender. The HBPUI/*o*-clay-silica hybrid films were obtained by casting the chain extender containing hybrid resins on a tin foil supported over a glass plate through manually driven square applicator in the presence of DBTL as catalyst and Tagostab as surfactant. The casted films were kept for about 20–25 days under the laboratory humidity condition for curing.[38,39] The absence of *NCO* peaks at 2270 cm^{-1} and the appearance of urethane/urea as well as imide peaks at 1540, 1780, and 1380 cm^{-1} in FTIR spectra of different HBPUI/*o*-clay-silica hybrid films confirms the completion of the curing reaction through the formation of urethane linkages. The reaction conditions and the steps involved in the synthesis of HBPUI/*o*-clay-silica hybrid coating is shown in Scheme 2, while their sample codes and chemical compositions are given in Table I.

RESULTS AND DISCUSSION

Powder XRD analysis

The overlapped XRD spectra of pristine and *o*-clays are shown in Figure 1. The peak at 13.5Å (1.35 nm) corresponds to basal plane spacing of the unmodified MMT clay shifting to <2 value after modification with different cationic surfactants, suggesting the intercalation of long chain cationic surfactants into the clay gallery. The extent of intercalation is highest in case of K10-TBHPB (d = 2.30 nm) and

TABLE I
Sample Codes and Chemical Compositions of Different HBPUI/*o*-Clay-Silica Hybrid Coatings

Sample code	Chemical compositions of the formulations
HBPUI-CTAB-Si-1%	HBP-G1 + HMDI + K10-CTAB-Si-1% + NHTM
HBPUI-CTAB-Si-3%	HBP-G1 + HMDI + K10-CTAB-Si-3% + NHTM
HBPUI-CTAB-Si-5%	HBP-G1 + HMDI + K10-CTAB-Si-5% + NHTM
HBPUI-CTAB-Si-7%	HBP-G1 + HMDI + K10-CTAB-Si-7% + NHTM
HBPUI-CTAB-Si-10%	HBP-G1 + HMDI + K10-CTAB-Si-10% + NHTM
HBPUI-TBHPB-Si-1%	HBP-G1 + HMDI + K10-TBHPB-Si-1% + NHTM
HBPUI-TBHPB-Si-3%	HBP-G1 + HMDI + K10- TBHPB-Si-3% + NHTM
HBPUI-TBHPB-Si-5%	HBP-G1 + HMDI + K10- TBHPB-Si-5% + NHTM

lowest for K10-CTAB (d = 1.81 nm), suggesting a monolayer type of arrangement for CTAB-modified samples and a bilayer to pseudo trilayer or paraffin-type arrangement for TBHPB-modified sample, respectively.[40] The monolayer type arrangement in K10-CTAB suggests that a large portion of ammonium modifier is associated with the external surface of MMT, while the bilayer to pseudo trilayer type arrangement in case of TBHPB-modified system suggests considerable swelling of the clay gallery as also reflected in the thermal behavior of the hybrid coatings.

FTIR analysis

The overlapped FTIR spectra of pristine, organically modified and different siloxane-grafted clays are shown in Figure 2(a). Compared with unmodified clay, APTMS-grafted samples exhibit extra peaks at 2930, 1490, 1330, and 1556 cm^{-1} along with a decrease in intensity[41] of the —OH stretching band at 3656 cm^{-1} The absorption band at 970 and 536 cm^{-1} are assigned to stretching of terminal Si—OH groups and Al—O—Si deformation signal becomes stronger in the spectra of silane-modified *o*-clay samples, suggesting the successful grafting of APTMS

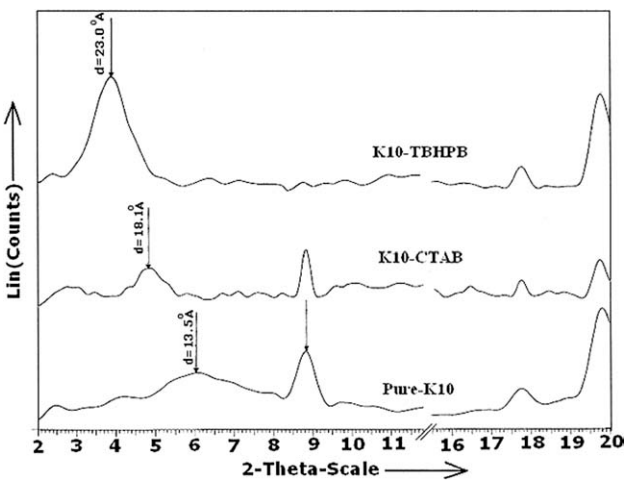

Figure 1 XRD spectra of pure and different organically modified K10-clays in 2θ range of 2–20.

onto *o*-clay surface as accompanied by the consumption of surface Al(OH) groups. The representative overlapped FTIR spectra of different HBPUI/*o*-clay-silica hybrid films are shown in Figure 2(b). The characteristic peaks at 1780, 1380, 1120, and 720 cm^{-1} in the overlapped FTIR spectra were assigned to the carbonyl stretching vibrations of imide I, imide II, imide III, and imide IV groups, respectively. This result confirms the insertion of imide groups into the polymer backbone. However, the bands at 1078, 1728, 1540, 2921, 2862, and 3425 cm^{-1} are due to the Si—O—Si stretching of clay or siloxane unit, hydrogen-bonded urethane carbonyl (—C=O), secondary urethane amide group (—C—NH), asymmetric and symmetric —C—H stretching vibration and H-bonding —NH group of the urethane molecule, respectively. The combined FTIR data confirm the formation of HBPUI/*o*-clay-silica hybrid coatings.

In case of PU, the hydrogen-bonding donor sites are the —NH groups of urethane linkages and hydrogen-bond acceptors may be either carbonyl group of the hard urethane/imide or soft ester segments. The FTIR peak deconvolution of —C=O and —NH zone, for HBPUI-CTAB-Si-3% and HBPUI-CTAB-Si-5% sample in the range of 1600–1800 and 3000–3800 cm^{-1}, are shown in Figure 2(c,d), respectively. For this, a flat baseline was chosen and the second derivative of the spectra in $\nu_{C=O}$ and ν_{N-H} zones was used to find the number of Gaussian peaks with the fitting correlation coefficients >0.99. The peak values at 1777, 1737, 1716, and 1666 cm^{-1} are assigned to free imide, hydrogen-bonded imide, free urethane, and bonded urethane, respectively. The peak area of free and hydrogen-bonded imide and urethane/urea, —C=O groups [Fig. 2(c)] suggests a higher contribution of hydrogen-bonded structure for HBPUI-CTAB-Si-5%, due to more interchain association through hydrogen-bonding between clay hydroxyl groups and carbonyl group of urethane/imide hard segments, which are consistent with our earlier published reports.[42,43] Since we could not separate the free and hydrogen-bonded —C=O groups, of the ester and urea function and hence, we assign their positions at 1716 and 1666

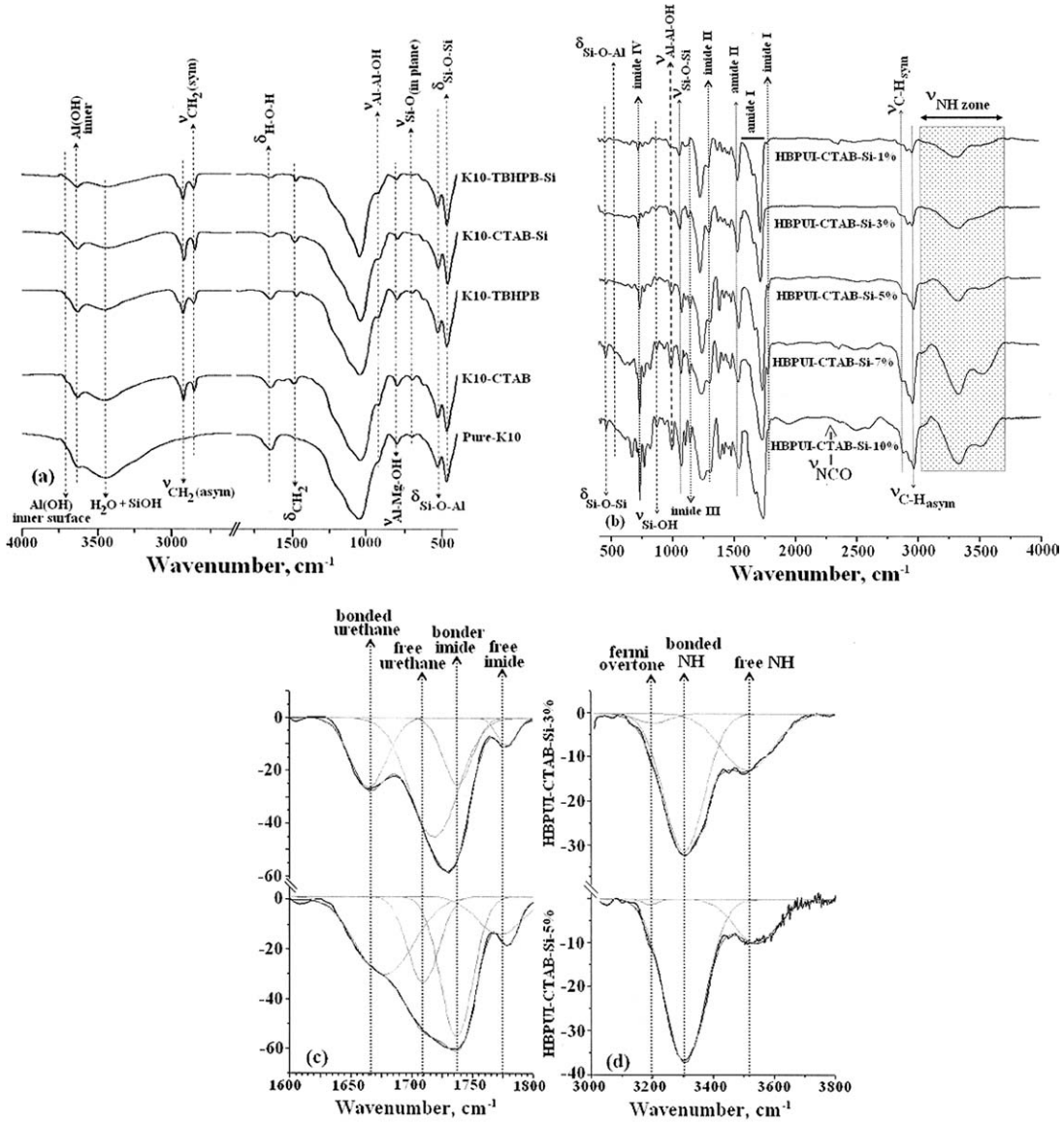

Figure 2 (a) FTIR spectra of pure K10-clay along with different organically modified and siloxane-grafted *o*-clays in the range 400–4000 cm^{-1}; (b) The overlapped FTIR spectrum of different HBPUI/*o*-clay-silica hybrid coatings in the range 400–4000 cm^{-1}; (c–d) Representative FTIR peak deconvolution of (c) —C=O, zone and (d) —NH, zone of HBPUI-CTAB-Si-3% and HBPUI-CTAB-Si-5% hybrid coatings in the range of 400–4000 cm^{-1}.

cm^{-1} along with the free and hydrogen-bonded urethane —C=O groups, respectively. The —C=O zone deconvolution data (not displayed) of different HBPUI/*o*-clay-silica hybrid samples suggests that the peak contribution from hydrogen-bonded —C=O from amide, imide/ester groups is highest for HBPUI-CTAB-Si-10%. In a similar way, the deconvoluted FTIR spectra of —NH stretching region [as shown in Fig. 2(d)], indicates that three peaks at 3503, 3302, and 3197 cm^{-1} are assigned to free —NH, hydrogen-bonded —NH (between the O=C— group of the hard segments), and overtone due to Fermi resonance, respectively.[44] Thus, FTIR deconvolution result suggests the presence of more hydrogen-bonded structures (see the deconvoluted peak area) in case of higher silane-grafted *o*-clay containing hybrid coatings viz., HBPUI-CTAB-Si-5%. The —NH deconvolution result also shows similar trends to that of —C=O zone deconvolution.

Thermogravimetric analysis of the coatings

TGA thermograms of different HBPUI/*o*-clay-silica hybrid films with increasing the content of silane-modified *o*-clay is shown in Figure 3(a), while their corresponding thermal data are given in Table II. Figure 3(a), indicates the presence of two major steps of decomposition, with the initial step of degradation occurring between 200 and 370°C. The first decomposition step is primarily due to the

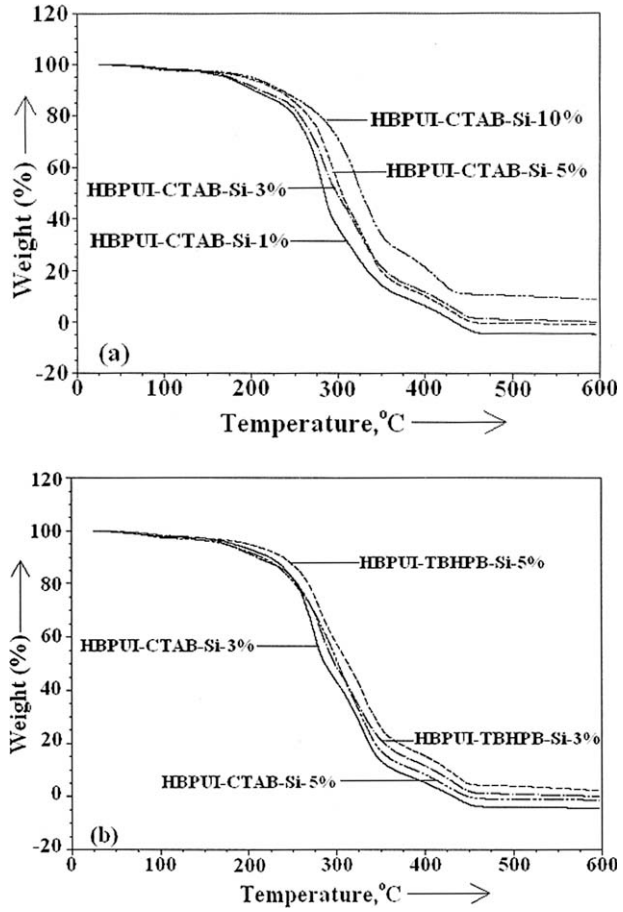

Figure 3 (a) Representative TGA curves of different silane-grafted *o*-clay based HBPUI/*o*-clay-silica hybrid films; (b) Representative TGA thermograms of different silane-grafted phosphonium and ammonium surfactant-modified *o*-clay based HBPUI/*o*-clay-silica hybrid films.

decomposition of hard segments, while the second stage is due to soft polymer degradation. TGA data as given in Table II, suggests the increasing order of thermal stability for hybrid films, and the order is as follows: HBPUI-CTAB-Si-1% < HBPUI-CTAB-Si-3% < HBPUI-CTAB-Si-5% < HBPUI-CTAB-Si-10%. For instance, T_{1ON} and 50% weight loss temperature (T_{d50}) for HBPUI-CTAB-Si-1%, HBPUI-CTAB-Si-3%, and HBPUI-CTAB-Si-5% are 189, 193, 210 and 295, 308, 309°C, respectively, probably due to the combined effect of two factors (i) polymer chain motions in silicate layers may be barred and limited, which increases the thermal stability[45,46] and (ii) the presence of high thermally stable Si—O—Si networks makes the path longer for escaping of volatiles generated during the initial stage of decomposition.[47,48] The representative TGA thermograms of surfactant-modified *o*-clay-based HBPUI/*o*-clay-silica films is shown in Figure 3(b). The obtained thermal data suggests higher thermal stability for phosphonium-modified films than their corresponding ammonium counterparts. For instance, T_{d10} and T_{d50} decomposition temperatures for HBPUI-CTAB-Si-3% and HBPUI-TBHPB-Si-3% are 224, 227, and 308, 310°C, respectively, suggesting the relatively loose arrangement[49] and lower polarity[50,51] of the of alkyl ammonium surfactants compared with the phosphonium counterpart.

DMTA and UTM analysis of the coatings

The tan δ versus temperature curves obtained by DMTA for different HBPUI/*o*-clay-silica hybrid films with increasing silane grafted *o*-clay content is shown in Figure 4(a), while their corresponding glass transition temperatures (T_g) and cross-link density (υ_e) values are displayed in Table III. The obtained result suggests an increasing trend of T_g values with increasing the silane-grafted *o*-clay content in the coating formulations. For instance, T_g and υ_e values at (T_g + 5)°C for HBPUI-CTAB-Si-1%, HBPUI-CTAB-Si-3% and HBPUI-CTAB-Si-5% are, 94.0, 100.2, 101.6°C and 1.94×10^4, 3.29×10^4, 3.38×10^4 mol/cm^3, respectively. This is due to the restriction of chain mobility, resulting from the relatively stronger hydrogen-bonding interaction between the polymer matrix and silicate layers of the silane-modified *o*-clay.[52] The DMTA profiles of E' and tan δ versus temperature curves for HBPUI-

TABLE II
Thermal Stability Data of Different HBPUI/*o*-Clay-Silica Hybrid Films

Sample codes	Onset decomposition temperature T_{1ON} (°C)	10% weight loss temperature T_{d10} (°C)	50% weight loss temperature T_{50d} (°C)
HBPUI-CTAB-Si-1%	189	205	295
HBPUI-CTAB-Si-3%	193	224	308
HBPUI-CTAB-Si-5%	210	230	309
HBPUI-CTAB-Si-7%	231	242	320
HBPUI-CTAB-Si-10%	233	246	325
HBPUI-TBHPB-Si-1%	202	211	286
HBPUI-TBHPB-Si-3%	207	227	310
HBPUI-TBHPB-Si-5%	219	241	213

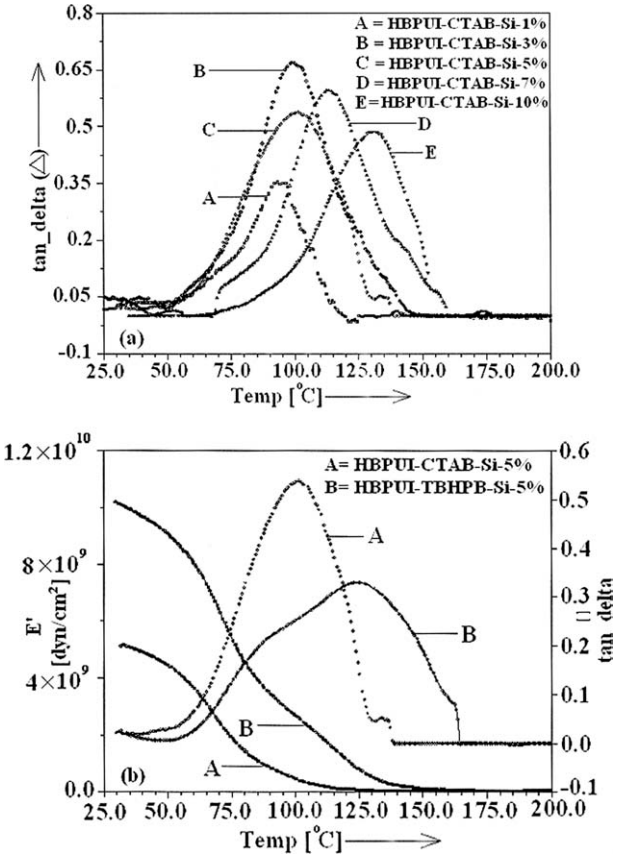

Figure 4 (a) DMTA profile of tan δ versus temperature curves of different silane-modified *o*-clay based HBPUI/*o*-clay-silica hybrid films; (b) Representative DMTA profiles of E' and tan δ versus temperature curves of different surfactant-modified *o*-clay based HBPUI/*o*-clay-silica hybrid films.

CTAB-Si-5% and HBPUI-TBHPB-Si-5% in the temperature range of 25–200°C are shown in Figure 4(b), and the study result suggest higher T_g and storage modulus values of phosphonium-modified hybrid coatings than the ammonium-based counterparts. This behavior might be due to the loose network arrangement of ammonium modifiers onto the surface of polymer, as supported by TGA data. The tensile data obtained for different HBPUI/*o*-clay-silica hybrid films with increasing silane-modified *o*-clay content is given in the Table IV. The result suggests an increase in tensile strength and a decrease in elongation at break with increasing the silane-grafted *o*-clay content. This could be attributed to the combined effects of (i) nano-reinforcement effect from silane-grafted *o*-clays, which restricts the macromolecular chain mobility through close packing arrangements and does not allow the polymer to stretch, thereby increases tensile strength and decreases elongation at break[53,54] and (ii) the formation of more number of polysilsesquioxane spheres through the stable Si—O—Si networks might increase the hardness of the coated film, thus increasing their tensile strengths.[55,56]

AFM analysis of the coatings

AFM was used to examine the dispersion of APTMS-grafted *o*-clays into the polymer matrix. The 1D and 3D AFM images of pure polymer and different APTMS grafted *o*-clay-based hybrid films is shown in Figure 5. The roughness data suggests varying surface roughness for different APTMS-grafted *o*-clay-based hybrid coatings, which decrease with increasing silane-modified *o*-clay content. For instance, root mean square roughness (R_q) values obtained for pure polymer, HBPUI-CTAB-Si-3%, and HBPUI-CTAB-Si-5% hybrid coatings are 0.121, 1.311, and 0.928 nm, respectively, confirming the dispersibility of APTMS-grafted *o*-clay particles into the polymer matrix increases (i.e., surface roughness decreases) with increasing silane-modified *o*-clay content of the coatings.[57] This effect is due to combined effect of higher reactivity of terminal amine groups (present in the APTMS-grafted *o*-clays) with PU prepolymer and improved hydrogen-bonding between the *o*-clay hydroxyl groups and urethane/urea or imide —C=O, groups.[58]

Contact angle measurement

The hydrophobicity of hybrid films with increasing *o*-clay content at different contact time was evaluated by contact angle measurement device. The droplets of distilled water were placed on different areas of the film surface using a micro-syringe and the mean reading was taken as the real value for contact angle. The variation of contact angles of different HBPUI/*o*-clay-silica hybrid films against wt % of silane-modified *o*-clay content is given in Table IV. The data suggests that contact angle increases with increasing silane-modified *o*-clay content at a particular contact time, while it decreases with increasing contact time for a particular wt % of

TABLE III
DMTA Data of Different HBPUI/*o*-Clay-Silica Hybrid Films

Sample codes	T_g (°C)	$E' \times 10^8$ [Pa] at $(T_g + 5)$°C	$\upsilon_C \times 10^4$ (mol/cm^3) at $(T_g + 5)$°C
HBPUI-CTAB-Si-1%	94.0	1.8	1.94
HBPUI-CTAB-Si-3%	100.2	3.1	3.29
HBPUI-CTAB-Si-5%	101.6	3.2	3.38
HBPUI-CTAB-Si-7%	113.4	3.5	3.59
HBPUI-CTAB-Si-10%	132.0	4.7	4.60
HBPUI-TBHPB-Si-1%	102.4	3.9	4.11
HBPUI-TBHPB-Si-3%	105.4	4.9	5.12
HBPUI-TBHPB-Si-5%	124.1	5.7	5.68

TABLE IV
UTM and Contact Angle Data of Different HBPUI/*o*-Clay-Silica Hybrid Films

Sample codes	Initial contact angle	Contact angle after 20 min	Tensile strength (MPa)	Maximum displacement (mm)	Elongation at break (%)
HBPUI-CTAB-Si-1%	58	44	5.6	28.4	56.8
HBPUI-CTAB-Si-3%	63	47	8.7	25.8	51.6
HBPUI-TBHPB-Si-3%	72	53	12.4	23.1	46.2
HBPUI-CTAB-Si-5%	80	61	16.6	12.9	25.8
HBPUI-TBHPB-Si-5%	86	63	18.3	9.6	19.2
HBPUI-CTAB-Si-7%	92	68	21.2	3.8	7.6
HBPUI-CTAB-Si-10%	87	70	23.1	3.1	6.2

silane-modified *o*-clay loading. However, extent of reduction in contact angle with increasing contact time is dependent on *o*-clay content, which increases slowly at higher wt % of silane-modified *o*-clay loading.[57] This could be due to decrease in surface polarity because of the formation of more polar cross-linked structures in the bulk[59] and the enrichment of intercalating agents at the surface of the film due to their higher migration aptitude.[60] Thus, the surface hydrophobicity increases with increasing silane-modified *o*-clay content of the coating formulation.

CONCLUSIONS

In this research, novel HBPUI/*o*-clay-silica hybrid coatings were prepared and characterized for their possible applications as coatings materials. It was found that the *o*-clay was successfully inserted into the K10-clay gallery by clay intercalation process and also the APTMS moiety was further grafted successfully into the *o*-clay surface. The TGA study reveals higher thermal stability for the phosphonium modifier (TBHPB)-based HBPUI/*o*-clay-silica hybrid films than their corresponding ammonium counterparts (CTAB) and it increases with increasing the silane-modified *o*-clay content. DMTA suggests that the storage modulus (E') at room temperature, glass transition temperature (T_g), and cross-link density, all increased with increasing the silane-modified *o*-clay content. AFM indicates better dispersibility of silane-modified *o*-clays into the PU matrix due to the favorable chemical interaction, which increases (i.e., surface smoothness increases) with increasing content of APTMS-grafted *o*-clay in the hybrid coatings. UTM and contact angle data suggests increased tensile strength and better hydrophobicity character for

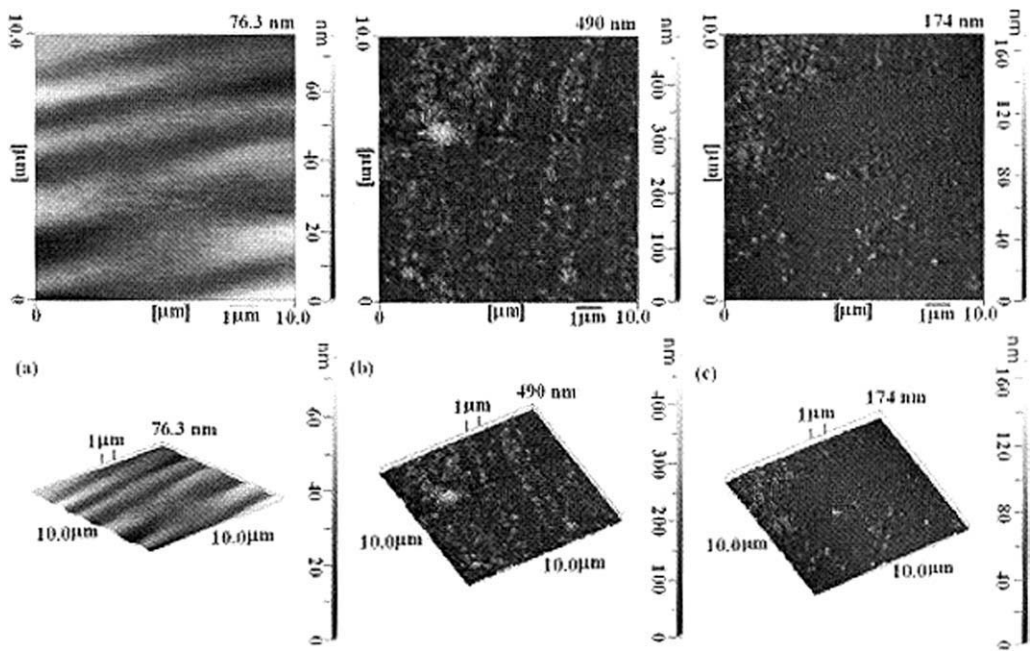

Figure 5 Representative 1D and 3D AFM images of (a) the pure polymer, (b) HBPUI-CTAB-Si-3%, and (c) HBPUI-CTAB-Si-5% hybrid films in a scan resolution of 10 μm.

the higher silane-modified *o*-clay containing hybrid coatings. Hence, this study can be used as guideline for the design and development of hybrid nanocomposite coatings for optically active films, contact lenses, corrosion resistance coating, flame retardancy coating, abrasion resistant coating, and coil coating applications.

The author, A. K. Mishra, thank Council of Scientific and Industrial Research (CSIR, New Delhi, India) for awarding the research fellows. T. M. Aminabhavi thank CSIR [21/(0760)/09/EMR-II], New Delhi, India for awarding Emeritus Scientist.

References

1. Masiulanis, B.; Zielinski, R. J Appl Polym Sci 1985, 30, 2731.
2. Dieterich, D. Prog Org Coat 1981, 9, 281.
3. Asif, A; Huang, C.; Shi, W. Polym Adv Technol 2003, 14, 609.
4. Liao, D. C.; Heich, K. H. J Polym Sci Part A: Polym Chem 1994, 32, 1665.
5. Tomalia, D. A.; Naylor, A. M.; Goddhard, W. A. Angew Chem 1990, 29, 138.
6. Kim, Y. H. J Polym Sci Part A: Polym Chem 1998, 36, 1685.
7. Voit, B. J Polym Sci Part A: Polym Chem 2000, 38, 2505.
8. Malmstrom, E.; Hult, A. Macromolecules 1996, 29, 1222.
9. Jung, J. C.; Park, S. B. J Polym Sci Part A: Polym Chem 1996, 34, 357.
10. Ghatge, N. D.; Mulik, U. P. J Polym Sci Part A: Polym Chem 1980, 18, 1905.
11. Gao, F.; Schricker, S. R.; Tong, Y.; Culbertson, B. M. J Macromol Sci Pure Appl Chem A 2002, 39, 267.
12. Asif, A.; Shi, W. Eur Polym Mater 2003, 39, 933.
13. Abdalla, M. O.; Dean, D.; Campbell, S. Polymer 2002, 43, 5887.
14. Lan, T.; Kaviratna, P. D.; Pinnavaia, T. J Chem Mater 1995, 7, 2144.
15. Ma, J.; Zhang, S.; Qi, Z. J Appl Polym Sci 2001, 82, 1444.
16. Chen, T. K.; Tien, Y. I.; Wei, K. H. Polymer 2000, 41, 1345.
17. Yeh, J. M.; Liou, S. J.; Lin, C. Y.; Cheng, C. Y.; Chang, Y. W. Chem Mater 2002, 14, 154.
18. Gorrasi, G.; Tortora, M.; Vittoria, V. J Polym Sci Part B: Polym Phys 2005, 43, 2454.
19. Devaux, E.; Rochery, M.; Bourbigot, S. Fire Mater 2002, 26, 149.
20. Goda, H.; Frank, C. W. Chem Mater 2001, 13, 2783.
21. Yao, K. J.; Song, M.; Hourston, D. J.; Luo, D. Z. Polymer 2002, 43, 1017.
22. Chang, J. H.; An, Y. U. J Polym Sci Part B: Polym Phys 2002, 40, 670.
23. Xu, R.; Manias, E.; Snyder, A. J.; Runt, J. Macromolecules 2001, 34, 337.
24. Gilman, J. W. Appl Clay Sci 1999, 15, 31.
25. Lebaron, P.C.; Wang, Z.; Pinnavaia, T. J Appl Clay Sci 1999, 15, 11.
26. Petrovic, Z. S.; Javni, I.; Waddon, A.; Banhegyi, G. J Appl Polym Sci 2000, 76, 133.
27. Wang, Z.; Pinnavaia, T. J Chem Mater 1998, 10, 3769.
28. Zilg, C.; Thomann, R.; Mulhaupt, R.; Finter, J. Adv Mater 1999, 11, 49.
29. Chattopadhyay, D. K.; Mishra, A. K.; Sreedhar, B.; Raju, K. V. S. N. Polym Degrad Stab 2006, 91, 1837.
30. Slavov, S. V.; Chuang, K. T.; Sanger, A. R. J Phys Chem 1996, 100, 16285.
31. Braggs, B.; Fornasiero, D.; Raltston, J.; Smart, R. St. Clays Clay Miner 1994, 42, 123.
32. Gryshchuk, O.; Jost, N.; Karger, K. J Polymer 2002, 43, 4763.
33. Zou, J.; Shi, W.; Hong, X. Compos Part A 2005, 36, 631.
34. Schrotter, J. C.; Smaihi, M.; Guizard, C. J Appl Polym Sci 1996, 61, 2137.
35. Chiu, Y. S.; Liu, Y. L.; Wei, W. L.; Chen, W. Y. J Polym Sci Part A: Polym Chem 2003, 41, 432.
36. Sabzi, M.; Mirabedini, S. M.; Mehr, J. Z.; Atai, M. Prog Org Coat 2009, 65, 222.
37. Goswami, A.; Singh, A. K. React Funct Polym 2004, 61, 255.
38. Wei, W. J.; Guo, Z. R.; Zhang, Y. F.; Pan, E. L. J Appl Polym Sci 2002, 84, 1346.
39. Kurita, K.; Imajo, H.; Iwakura, Y. J Polym Sci Part A: Polym Chem 1979, 17, 1619.
40. Hedley, C. B., Yuan, G.; Theng, B. K. G. Appl Clay Sci 2007, 35, 180.
41. Capozzi, C. A.; Condrate, R. A.; Pye, L. D.; Hapannowicz, R. P. Mater Lett 1994, 18, 349.
42. Pattanayak, A.; Jana, S. C. Polymer 2005, 46, 3275.
43. Dai, X.; Xu, J.; Guo, X.; Lu, Y.; Shen, D.; Zhao, N.; Xiangdong, L.; Zhang, X. Macromolecules 2004, 37, 5615.
44. Romanova, V.; Begishev, V.; Karmanov, V.; Kondyurin, A.; Maitz, M. F. J Raman Spectr 2002, 33, 769.
45. Kumari, S.; Mishra, A. K.; Krishna, A. V. R.; Raju, K. V. S. N. Prog Org Coat 2007, 60, 54.
46. Liu, P.; Song, J.; He, L.; Liang, X.; Ding, H.; Li, Q. Eur Polym Mater 2008, 44, 940.
47. Liu, Y.; Ni, Y.; Zheng, S. Macromol Chem Phys 2006, 207, 1842.
48. Pyun, J.; Matyjaszewski, K. Chem Mater 2001, 13, 3436.
49. Xi, Y. F.; Zhou, Q.; Frost, R. L.; He, H. P. J Collid Interface Sci 2007, 311, 347.
50. Ghasemi, H.; Carreau, P. J.; Kamal, M. R.; Calderon, J. U. Polym Eng Sci, Published online; DOI 10.1002/pen.21874, 2011.
51. Kamal, M. R.; Calderon, J. U.; Lennox, R. B. J Adhes Sci Technol 2009, 23, 663.
52. Finnigan, B.; Martin, D.; Halley, P. Truss, R.; Campbell, K. Polymer 2004, 45, 2249.
53. Mishra, A. K.; Allauddin, S.; Radhika, K. R.; Narayan, R.; Raju, K. V. S. N. Polym Adv Technol 2011, 22, 882.
54. Svoboda, P.; Zeng, C.; Wang, H. L.; Lee, J.; Tomasko, D. L. J Appl Polym Sci 2002, 85, 1562.
55. Cho, J. W.; Lee, S. H. Eur Polym Mater 2004, 40, 1343.
56. Nomura, Y.; Sato, A.; Sato, S.; Mori, H.; Endo, T. J Polym Sci Part A: Polym Chem 2007, 45, 2689.
57. Huang, K. Y.; Weng, C. J.; Lin, S. Y.; Yu, Y. H.; Yeh, J. M. J Appl Polym Sci 2009, 112, 1933.
58. Xiong, J.; Zheng, Z.; Jiang, H.; Ye, S.; Wang, X. Compos Part A 2007, 38, 132.
59. Mishra, A. K.; Jena, K. K.; Raju, K. V. S. N. Prog Org Coat 2009, 64, 47.
60. Deng, X.; Liu, F.; Luo, Y.; Chen, Y.; Jia, D. Prog Org Coat 2007, 60, 11.